Journal of Glaciology

Article

Cite this article: Nyamgerel Y, Han Y, Kim S, Hong S-B, Lee J, Hur SD (2020). Chronological characteristics for snow accumulation on Styx Glacier in northern Victoria Land, Antarctica. *Journal of Glaciology* **66**(260), 916–926. https://doi.org/10.1017/jog.2020.53

Received: 30 November 2019
Revised: 25 June 2020
Accepted: 26 June 2020
First published online: 26 August 2020

Key words:
Annual layer counting; ionic species; snow accumulation; stable water isotopes; Styx Glacier

Author for correspondence:
Jeonghoon Lee,
E-mail: jeonghoon.d.lee@gmail.com

cambridge.org/jog

Chronological characteristics for snow accumulation on Styx Glacier in northern Victoria Land, Antarctica

Yalalt Nyamgerel[1,2], Yeongcheol Han[2], Songyi Kim[1,2], Sang-Bum Hong[2], Jeonghoon Lee[1] and Soon Do Hur[2]

[1]Department of Science Education, Ewha Womans University, Seoul 120-750, Korea and [2]Division of Paleoenvironment, Korea Polar Research Institute, Incheon, 21990, Korea

Abstract

Under the potential to reconstruct the past climatic and atmospheric conditions from a deep ice core in the coastal Antarctic site (Styx Glacier), an 8.84 m long firn core (73°50.975′ S, 163° 41.640′ E; 1623 m a.s.l.) was initially studied to propose a reliable age scale for the local estimation of snow accumulation rate. The seasonal variations of $\delta^{18}O$, methanesulfonic acid (MSA) and non-sea-salt sulfate ($nssSO_4^{2-}$) were used for the firn core dating and revealed 25 annual peaks (from 1990 to 2014) with volcanic sulfate signal. The observed declining trend in annual accumulation rate with a mean value of 146 ± 60 kg m^{-2} a^{-1} is likely to be linked to the changes of sea-ice extent in the Ross Sea region. Moreover, the temporal variation of the annual mean $\delta^{18}O$, an annual flux of MSA and $nssSO_4^{2-}$ also likely to be under the influence of ice-covered and open water area. This study suggests a potential to recover past changes in an oceanic environment and will be useful for the interpretation of the long ice core drilled at the same site.

1. Introduction

Ice core chronology is an initial and essential step for the interpretation of the past records of climate, environment and atmospheric circulation from polar ice cores (Legrand and Mayewski, 1997; Traversi and others, 2004; Sinclair and others, 2010; Furukawa and others, 2017). A precise chronology provides an accurate quantification of snow accumulation rate in sub-annual and annual scales which is an important measure to surface mass-balance studies (Frezzotti and others, 2007; Rignot and others, 2011). Associated to the large spatial variability in Antarctic snowfall (Anschütz and others, 2011), the local estimation of snow accumulation rate is vital for the coastal Antarctic mass balance (Krinner and others, 2007), assessment of climate models, satellite measurements (Stenni and others, 2000; Goursaud and others, 2017) and the response of climate and environmental changes on polar ice sheet (Stenni and others, 2000; Sinclair and others, 2010; Kwak and others, 2015).

Age dating of firn cores has commonly been done by counting the seasonal signals of its stable water isotopic compositions ($\delta^{18}O$ and δD) and ionic species (e.g. Udisti, 1996; Wagenbach and others, 1998; Kreutz and others, 1999; Udisti and others, 1999; Delmotte and others, 2000; Stenni and others, 2000; Rhodes and others, 2012; Markle and others, 2012; Caiazzo and others, 2016; Goursaud and others, 2019). In coastal Antarctica, distinguishable seasonal signal of isotopic composition is trapped in snow layers and can be interpreted based on the conventional correlation of $\delta^{18}O$ (or δD) and air temperature (e.g. Dansgaard, 1964; Jouzel and others, 1997), coupled with the seasonal changes of sea-ice extent (SIE) (Bromwich and Weaver, 1983; Noone and Simmonds, 2004; Rhodes and others, 2012; Tuohy and others, 2015; Holloway and others, 2016). Moreover, the peak values of $CH_3SO_3^-$ (methanesulfonic acid [MSA]) and non-sea-salt sulfate ($nssSO_4^{2-}$) illustrate noticeable peaks during spring and summer in the northern Victoria Land (e.g. Udisti and others, 1998; Rhodes and others, 2012; Becagli and others, 2016).

Due to the short-term and sparse instrumental data (e.g. Stenni and others, 2000; Tuohy and others, 2015, Jones and others, 2016), trying to capture the high-spatial variability of the vast Antarctic continent (Masson-Delmotte and others, 2008), more proxy records with sufficient resolution are still necessary to be reconstructed (Goursaud and others, 2019). Particularly at coastal sites, there is a need to improve the interpretation of past environmental and climate records (Dansgaard, 1964; Stenni and others, 2000, 2017; Krinner and others, 2007; Jouzel and Masson-Delmotte, 2010; Tuohy and others, 2015; Goursaud and others, 2019). Accordingly, the northern Victoria Land is characterized by less available data and large variability in temperature (Yang and others, 2018). The combination of the high-altitude Transantarctic Mountains and the low-altitude coastal areas means that this site is a potential location for the study of air mass transport at both the regional and global scale (Udisti and others, 1998). Moreover, a strong influence from marine sources also enhances the particular interest to investigate the variability of SIE (Drewry and others, 1982; Han and others, 2015; Kwak and others, 2015; Thomas and others, 2019). In addition, the previous studies showed a relatively higher accumulation that ranged from 203 to 226 kg m^{-2} a^{-1} in Styx Glacier (Stenni and others, 2000; Kwak and others, 2015), thus, the site is assumed to provide better annual signals of proxy records with negligible effects

of post-deposition noise (Maggi and others, 1998; Frezzotti and others, 2007; Goursaud and others, 2019).

As a part of the ongoing research at Jang Bogo Korean research station focused on reconstructing past climate with a focus on changes in SIE, two cores (210.5 and 8.84 m long) were obtained from the Styx Glacier during 2014–15 austral summer. The 210.5 m long ice core (Styx-M) is approximately estimated to cover the time period back to >2 ka (Han and others, 2015; Yang and others, 2018). To interpret the long ice core (Styx-M) and for accurate dating, the isotopic and ionic composition of the less consolidated snow layers in the firn core (Styx-B) are important. In this study, the chronological characteristics of 8.84 m long firn core (Styx-B) was discussed by evaluating the seasonal variations of the isotopes ($\delta^{18}O$ and δD) and major ionic species (Na^+, K^+, Mg^{2+}, Ca^{2+}, MSA, Cl^- and SO_4^{2-}). The correlation and principal component analyses were applied to characterize the record of isotopes and ionic species. The seasonal signals of the $\delta^{18}O$ and δD, $nssSO_4^{2-}$ and MSA were detected as already done in earlier studies (e.g. Udisti, 1996; Udisti and others, 1998; Stenni and others, 2000; Kwak and others, 2015; Caiazzo and others, 2016) and the annual mean snow accumulation rates were estimated. The mean accumulation rate was compared with the estimation by firn densification models (Herron and Langway, 1980; Morris, 2018). More reliably interpreting this core is made possible by comparison with instrumental data and the known climate events in recent years. This study will extend the previous records in this site (Udisti and others, 1998; Stenni and others, 2000; Traversi and others, 2004) and will be useful for the interpretation of the long ice core drilled at same site to represent the historical changes of oceanic (e.g. sea ice) and atmospheric environment in this region.

2. Materials and methods

2.1. Study area

The drilling site (73°50.975′ S, 163°41.640′ E; 1623 m a.s.l.) is situated on the Styx Glacier (150 km^2 plateau area) in the northern Victoria Land, East Antarctica, which is 85 km north of the Jang Bogo Station and ~60 km from the western coast of the Ross Sea (Fig. 1). During the Korean ice core drilling program (2014–15), the firn core (Styx-B) was drilled from the adjacent position (at a distance of ~100 m) of the longer ice core (Styx-M) by Korea Polar Research Institute (KOPRI). The annual mean temperature was −32.5°C, based on the 15 m depth borehole temperature measurement (Yang and others, 2018) and a horizontal ice flow was estimated to be ~0.9 m a^{-1}, and an ice thickness was determined to be 550 m by using a ground-penetrating radar (Hur, 2013).

Air mass mainly originates from the low-pressure center locally formed over the Ross Sea (Drewry and others, 1982; Scarchilli and others, 2011; Sinclair and others, 2012) with the prevailing southerly and southwesterly wind in this region (Udisti and others, 1999). During the period of 1980–2010, the sources from oceanic/West Antarctic (57.4%) and continental/East Antarctic (42.6%) were suggested as the dominant source to Ross Sea region (Markle and others, 2012). Stenni and others (2000) indicated that this region is a flat area with well-preserved snow layers, accompanying by a minimal effect from katabatic wind/existence of modest snowdrifts and absence of melting of ice layers (Udisti and others, 1998). Moreover, the accumulation rate is relatively high in this region (Stenni and others, 2000; Han and others, 2015) with respect to other inland Antarctic sites (e.g. Wagnon and others, 1999; Traversi and others, 2000). These features support the correct detection of the seasonal signals, because the high thickness of the annual snow layer prevents the uncertain stratum of snow that may result from the diffusion of isotopic components (Hoshina and others, 2016).

2.2. Sampling and analysis

The firn core with an average diameter of 0.09 m (ranged from 0.092 to 0.096 m) was collected in 18 runs by a drilling system by Geo Tecs Co., Ltd, Japan (Han and others, 2015). The average length for each run was 0.51 m (ranged between 0.25 and 0.84 m). During sampling, the density was estimated by measuring the mass and dimensions of the firn core subsections. The samples were kept frozen in polyethylene plastic bags and transported to KOPRI in Korea. The samples were stored under −20°C temperature in a cold room prior to the isotopic and ionic analysis.

Inside the cold room, the external thin layers were removed and cut with an average length of 0.04 m for isotopic analysis. The subsampled ice samples were melted at room temperature (~20°C) in a clean room and filtered by a 0.45-μm PVDF syringe filter (Merck Millipore, USA) before being decanted into 2-mL glass vials (dried for over 72 h at 50°C). Isotopic measurements were performed on 227 samples by a cavity ring-down spectroscopy (L1102-i, L2130-i, L2140-i, Picarro Inc., USA) and calibrated by International Atomic Energy Agency standards including Vienna Standard Mean Ocean Water (VSMOW), Greenland Ice Sheet Precipitation and Standard Light Antarctic Precipitation. Moreover, an in-house reference standard (with the isotopic composition of −34.6 ± 0.07‰ for $\delta^{18}O$ and −272.4 ± 0.6‰ for δD, respectively), prepared by Antarctic snowmelt was measured in every ten samples to monitor the operation of the analyzer. Isotopic ratios were expressed by the comparison with the VSMOW standard in delta notation ($\delta^{18}O$ and δD) with the unit of per mil (‰) as described in the following equation:

$$\delta = \left(\frac{R_{sample} - R_{VSMOW}}{R_{VSMOW}}\right) \times 1000 \quad (1)$$

where R represents the ratio of heavy to light isotopes ($^{18}O/^{16}O$ and D/H) in the sample and VSMOW standard. Analytical reproducibility was better than 0.1 and 1‰ for $\delta^{18}O$ and δD, respectively. The deuterium excess (*d-excess*), which represents the deviation of the distribution of isotopic composition from the global meteoric waterline (GMWL), was estimated by using the equation: $d\text{-}excess = \delta D - 8 \times \delta^{18}O$ (Dansgaard, 1964).

Ionic species (Na^+, K^+, Mg^{2+}, Ca^{2+}, MSA, Cl^- and SO_4^{2-}) were simultaneously measured with an average depth resolution of 0.045 m (in 197 samples) by the two-channel ion chromatography system (ICS-200 and ICS-2100; Thermo Fisher Scientific Inc., USA) at KOPRI. Anions (MSA, Cl^- and SO_4^{2-}) were measured using a Dionex model ICS-2000 with an IonPac AS15 column and KOH eluent (6–55 mM). For the cation analysis (Na^+, Ca^{2+}, Mg^{2+} and K^+), a Dionex model ICS-2100 with an IonPac CS12A column and MSA eluent (20 mM) were used. The analytical detection limit, reproducibility and accuracy were 0.01–0.26 μg L^{-1}, 0.4–17.4% and 4.5–12.0% for cations and 0.02–0.26 μg L^{-1}, 0.1–27.6% and 1.3–5.6% for anions, respectively (Hong and others, 2012). The non-sea-salt (nss) proportion of the ions including K^+, Mg^{2+}, Ca^{2+}, Cl^- and SO_4^{2-} were calculated to disentangle the input from the sea salt (ss) aerosol by Eqn (2). The theoretical ratio of certain ions and Na^+ in sea water were used (Pilson, 2013). In this equation, Na^+ was considered to be solely supplied from a sea spray (Kuramoto and others, 2011):

$$nss[X] = tot[X] - (X/Na^+)_{sw} \times Na^+ \quad (2)$$

where X is the ion species and $(X/Na^+)_{sw}$ is the ratio of the certain ion and Na^+ in sea water. Similarly, the enrichment factor of SO_4^{2-} was estimated by dividing the ratio $(SO_4^{2-}/Na^+)_{sample}$ in the sample to the theoretical ratio in sea water $(SO_4^{2-}/Na^+)_{sw}$ (Pilson, 2013).

https://doi.org/10.1017/jog.2020.53 Published online by Cambridge University Press

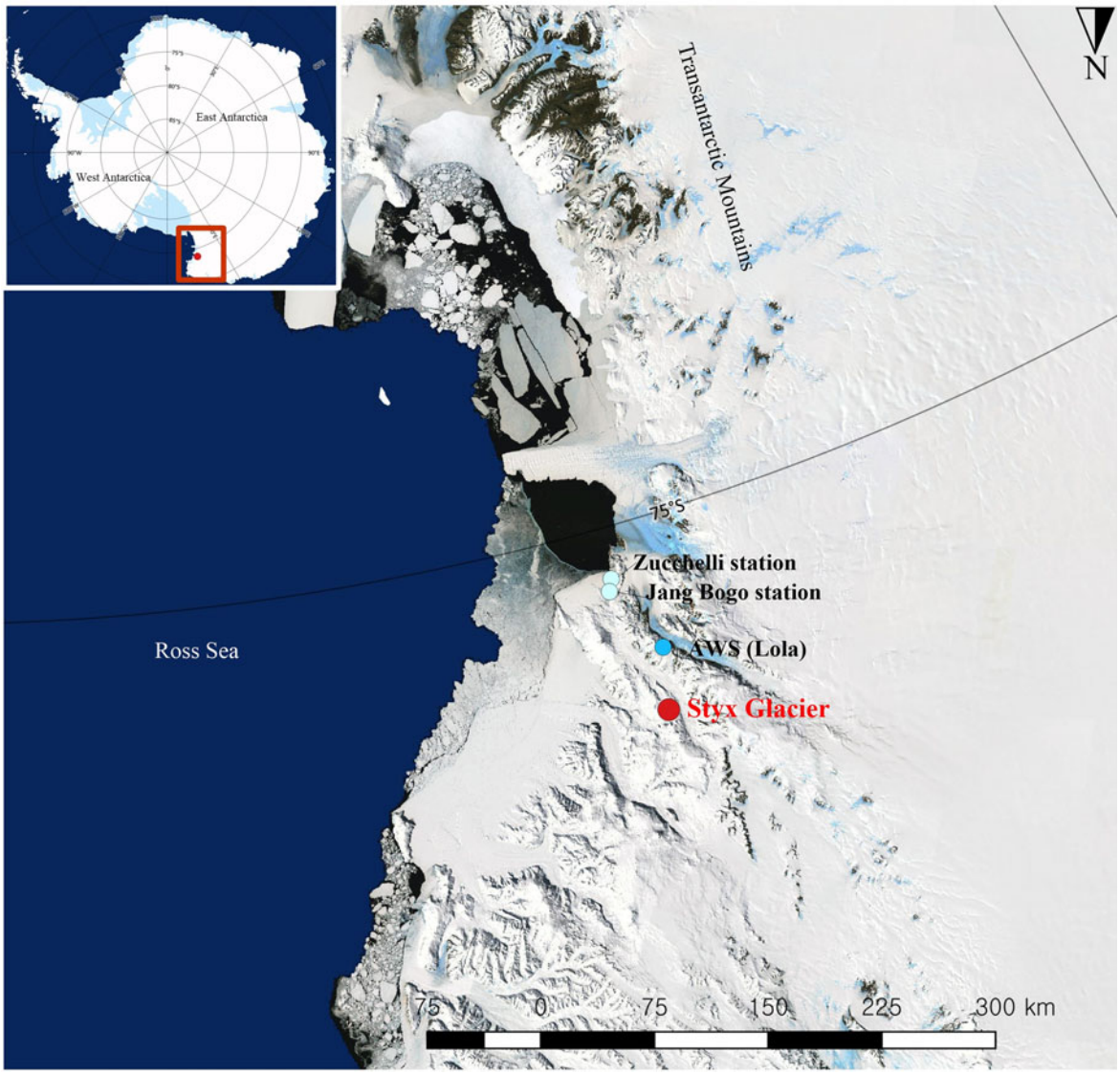

Fig. 1. The location of drilling site on Styx Glacier with South Korean Jang Bogo Research Station, Italian Mario Zucchelli Station and the nearest AWS (Lola) in Northern Victoria Land, East Antarctica.

2.3. Age–depth determination

Principal component analysis (PCA), the multivariate statistical technique, is applicable to classify the large dataset (e.g. Lee and others, 2008). Several studies have applied PCA to measure proxies for past atmospheric conditions from ice core records (e.g. Knüsel and others, 2005) and snow pits (Kwak and others, 2015). It was utilized to emphasize the dominant characteristics of isotopic and ionic values in same depth resolution of the firn core ($n = 197$) using JMP® statistical software. The inter-correlated variation, which represents the same atmospheric sources and common transport path (Knüsel and others, 2005; Kwak and others, 2015), is shown (Fig. 2) and assist the visual interpretation of the temporal signals by detecting the seasonal tendency.

The age determination was based on the seasonal peaks of $\delta^{18}O$ ($\delta^{18}O$ preferred and the correlation to δD is 0.99) with MSA and $nssSO_4^{2-}$ (e.g. Udisti and others, 1996; Kwak and others, 2015; Caiazzo and others, 2016), starting from the year of the drilling. The elevated values of $\delta^{18}O$ identified as midsummer (1 January) (e.g. Markle and others, 2012; Rhodes and others, 2012; Tuohy and others, 2015). Also, the age scale was adjusted with $nssSO_4^{2}$ signal of Pinatubo and Cerro Hudson volcanic eruption. The age for each sample was determined by the linear interpolation between subsequent two peaks. The number of samples per year ranged between 4 and 14 (averagely nine samples) and the annual accumulation rate was estimated in adjusted water-equivalent by multiplying its density.

Three stages of densification have been identified which reach 550, 820–840 and 917 kg m^{-3} in the first, second and third stages, respectively (Benson, 1962; Anderson and Benson, 1963; Herron and Langway, 1980). The density of the firn core (<500 kg m^{-3}) is lower than the critical density of 550 kg m^{-3}, thus only the first stage of the densification was considered. Within this stage, the firn becomes denser rapidly by the processes of grain-boundary sliding and grain growth due to the overlying weight of snow layers and the changes in temperature affects the densification rate (Herron and Langway, 1980). In the firn densification model 1 (M1) (Herron and Langway, 1980) and model 2 (M2) (Morris, 2018), the annual mean temperature of −32.5°C at 15 m borehole measurement was used (Yang and others, 2018). Age–depth calculation was performed with the mean accumulation rate of 150 kg m^{-2} a^{-1} which can be averaged from our annual layer counting (excluded a low value in 2014). The M2 used the different transition density

https://doi.org/10.1017/jog.2020.53 Published online by Cambridge University Press

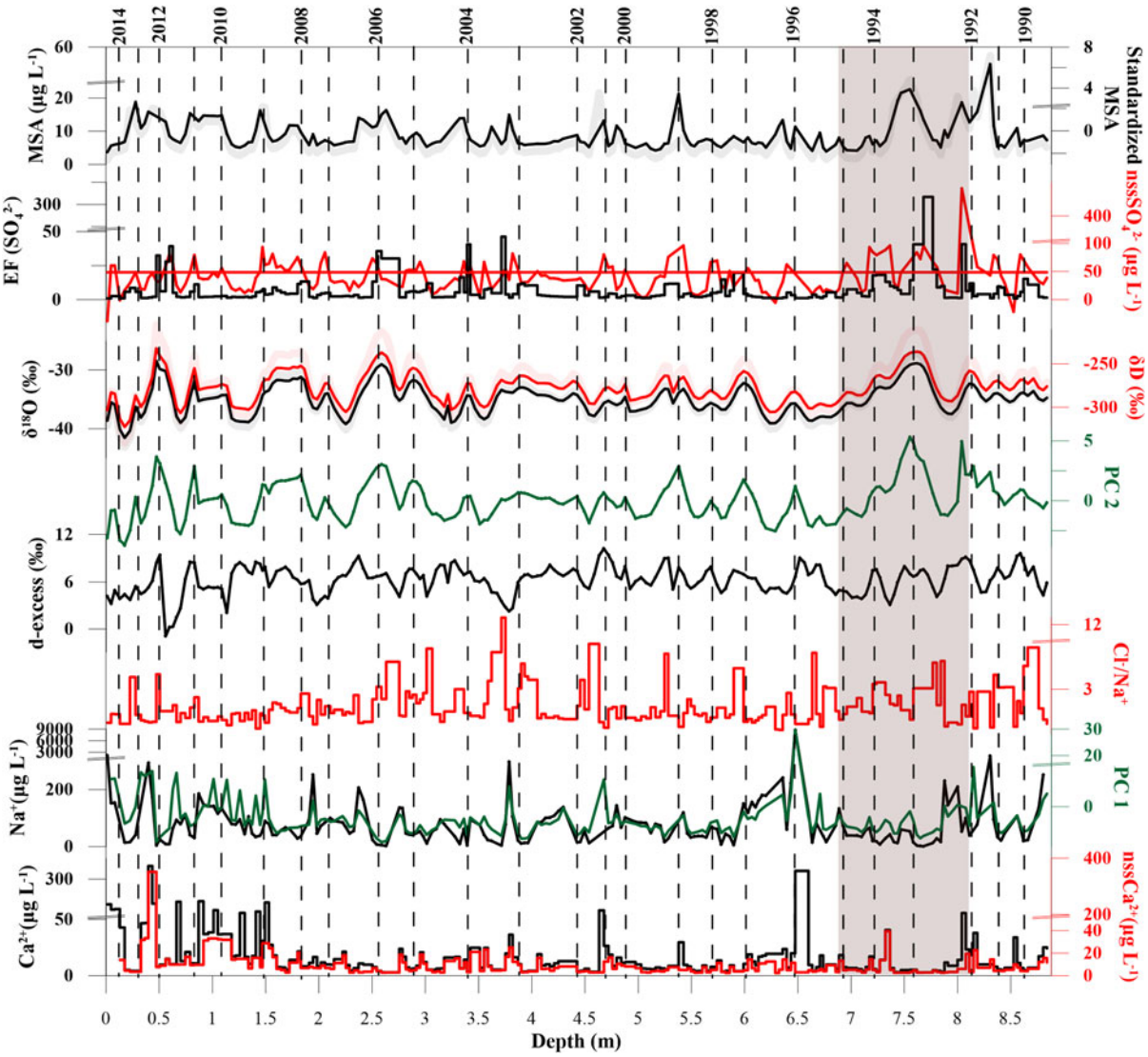

Fig. 2. Annual layer counting of the isotopic and ionic species with PC 1 and PC 2 scores, starting from the year of drilling (2014). The Cl^-, Mg^{2+} and K^+ are not shown in the figure because these are similar to Na^+ ($r > 0.99$), but the ratio of Cl^-/Na^+ is shown. Non-sea-salt portions are indicated for Ca^{2+}. The raw values (wide line) of $\delta^{18}O$, δD and MSA shown with standardized profile in thin line. Enrichment factor (EF) of $nssSO_4^{2-}$ was shown in black line and horizontal red line indicates the average $nssSO_4^{2-}$. Brown shading represents depth range to increased $nssSO_4^{2-}$ which indicate the period of Pinatubo and Cerro Hudson volcanic signals.

and scaling factor from the M1, which allowed modeling a smooth transition between the densification stages 1 and 2. The age scale by the annual layer counting was compared to the model results.

The forecast data (hourly average) of the precipitation (precipitation = total precipitation − evaporation) by the ERA-Interim reanalysis dataset produced by the European Centre for Medium-Range Weather Forecasts (ECMWF) in the nearest (~4 km) gridpoint (73° 52.30′ S, 163°37.30′ E) to the study area were selected and compared to our estimated snow accumulation rates (Dee and others, 2011). We also compared the annual mean isotopic composition ($\delta^{18}O$) with the instrumental temperature record from automatic weather station (Lola AWS), which locates ~40 km south of the site (http://www.climantartide.it) and 2–m temperature data from ERA-Interim reanalysis (Dee and others, 2011), and SIE (Parkinson and Cavalieri, 2012; Data archive at National Snow and Ice Data Center).

3. Results and discussion

3.1. Temporal variations of the isotopes and ionic species

The fluctuations in the concentrations of the ionic species with depth (depth is in snow depth) (Fig. 2) and the descriptive statistical parameters are displayed (Table 1). Strong positive correlations (r) were observed between Na^+ and other ionic species ($r > 0.9$ for K^+, Mg^{2+}, Cl^-, SO_4^{2-}, and $r = 0.5$ for Ca^{2+}, $n = 197$, $p < 0.001$). These species are the main components of sea-salt aerosols, which originated from the surrounding oceanic source (Piccardi and others, 1994; Traversi and others, 2004). The mean values of nss fractions of ionic species, including K^+ (19.2%), Mg^{2+} (19.1%) and Cl^- (25.1%) were lower than the Ca^{2+} (74.0%) and SO_4^{2-} (65.5%) (Table 1). The ion distributions were roughly right-skewed, related to the inconsistent increased sea-salt aerosols. An abrupt increase was noticed in the ionic concentrations, including Na^+, K^+, Mg^{2+}, Ca^{2+}, Cl^- and SO_4^{2-}, at a depth of 6.47 m. The highest fraction of sea-sourced Ca^{2+} (~99.9%) and the ratio of Cl^- to Na^+ (1.86), which is similar to the theoretical ratio of sea water (Pilson), observed at this depth, indicating the abnormal sea-salt aerosol input.

PCA was performed on the isotopic ($\delta^{18}O$, δD and *d-excess*) and ionic (Na^+, K^+, Mg^{2+}, Ca^{2+}, MSA, Cl^-, $ssSO_4^{2-}$ and $nssSO_4^{2-}$) values for same depth resolution of the firn core (n = 197). Principal component (PC) 1 explained 49.52% of the total variance with the strong loadings of the positively correlated sea-salt ions including Na^+, K^+, Mg^{2+}, Ca^{2+}, Cl^- and $ssSO_4^{2-}$ (Table 2).

https://doi.org/10.1017/jog.2020.53 Published online by Cambridge University Press

Table 1. Summary of statistics of water stable isotopes in ‰ ($n = 227$) and chemical species in $\mu g\,L^{-1}$ ($n = 197$) in the firn core

	Min	Max	Range	Mean	Median	Std. error	Std. deviation	Mean nss %
$\delta^{18}O$	−43.13	−26.70	16.43	−34.92	−34.85	0.21	3.13	–
δD	−340.63	−205.17	135.46	−273.11	−272.99	1.68	25.32	–
MSA	1.34	53.71	52.37	8.12	5.25	0.51	7.17	–
Cl^-	6.58	16 394.61	16 388.03	339.42	151.98	88.34	1239.98	25.1
SO_4^{2-}	13.38	2506.58	2493.20	91.63	65.80	13.43	188.53	65.5
Na^+	1.20	8802.32	8801.12	171.07	64.45	47.81	671.04	–[a]
K^+	0.43	373.13	372.70	7.38	2.61	2.04	28.60	19.2
Mg^{2+}	1.07	1042.42	1041.35	20.86	10.01	5.53	77.67	19.1
Ca^{2+}	2.73	362.57	359.83	26.97	9.91	3.64	51.08	74.0

[a]Assumed to be solely originated from sea spray.

Table 2. Loadings of 11 variables for first three principal components (PC) in the firn core with larger values highlighted in bold

	PC 1	PC 2	PC 3
$\delta^{18}O$	−0.12	**0.92**	−0.24
δD	−0.12	**0.93**	−0.17
d-excess	−0.03	0.33	**0.92**
MSA	0.15	**0.60**	0.09
Cl^-	**0.99**	−0.01	0.02
$ssSO_4^{2-}$	**0.99**	−0.01	0.02
$nssSO_4^{2-}$	0.33	**0.60**	0.01
Na^+	**0.99**	−0.01	0.02
K^+	**0.99**	−0.02	−0.01
Mg^{2+}	**0.99**	0.00	0.02
Ca^{2+}	**0.62**	−0.03	−0.19
Variance explained (%)	49.52	23.14	8.86
Cumulative percent (%)	49.52	72.66	81.52
Number of variables	197	197	197

This result highlights the dominant contribution of the oceanic source in line with other studies (Kwak and others, 2015). The second principal component (PC 2) has high loadings of $\delta^{18}O$, δD, $nssSO_4^{2-}$ and MSA, accounting for 23.14% of the total variance and indicates the identical seasonal nature of these variables. PC 1, PC 2 and PC 3 captured 81.52% of the total variance (Table 2), including 8.86% from PC 3 with high loading of *d-excess*. PCA classified the variables into species representing an input of sea-salt aerosol (PC 1) and species signing the seasonal cycle, related to the high temperature (PC 2). PC 2 score suggests the potential seasonal markers including $\delta^{18}O$, δD, $nssSO_4^{2-}$ and MSA (e.g. Stenni and others, 2000; Kwak and others, 2015).

3.1.1. Temporal variations of stable isotopic composition

The $\delta^{18}O$, δD and *d-excess* with the increasing depth were presented in Figure 2. The $\delta^{18}O$ (δD) values ($n = 227$) ranged from −43.13‰ (−340.6‰) to −26.70‰ (−205.2‰), with a mean value of −34.92‰ (−273.1‰), which were analogous to other records on the Styx Glacier (Stenni and others, 1999; Kwak and others, 2015). Moreover, mean $\delta^{18}O$ averaged from database, compiled in Masson-Delmotte and others (2008), showed similar values of −30.19‰ in the coastal Antarctic sites (~40–80 km from coast) and −30.91‰ in the sites, located in the elevation range between 1400 and 1800 m a.s.l. The isotopic compositions revealed maximum (summer) and minimum (winter) values with a distinct seasonal bias. Summer peak values (assumed as January) of $\delta^{18}O$ (δD) ranged between −36.50‰ (−287.2‰) and −27.22‰ (−210.9‰), respectively. There was not a clear increasing or decreasing trend in $\delta^{18}O$ (δD) in the whole record down to 8.84 m (Fig. 2). The seasonal pattern of $\delta^{18}O$ (δD) was used for stratigraphic dating with the assumption of less post-depositional effects due to the relatively high accumulation rate (e.g. Stenni and others, 2000; Kwak and others, 2015; Furukawa and others, 2017).

The linear relationship between $\delta^{18}O$ and δD appeared with a slope of 8.06 ($\delta D = 8.06 \times \delta^{18}O + 8.56$, $R^2 = 0.99$, $n = 227$, $p < 0.001$), which is fairly consistent with the GMWL ($\delta D = 8 \times \delta^{18}O + 10$) (Dansgaard, 1964). Masson-Delmotte and others (2008) reported a meteoric waterline ($\delta D = 7.75 \times \delta^{18}O - 4.93$, $R^2 = 0.98$, $n = 789$) at the continental scale, which is slightly different to our estimate. This negligible alteration of the slope leads us to assume that the accumulated snow layers are fairly well preserving the precipitation isotopic content with less influences by post-depositional processes, including temperature gradient metamorphism (Lee and others, 2010), diffusion process (Johnsen and others, 2000) and sublimation (e.g. Steen-Larsen and others, 2014).

The slope in summer (8.91) was larger with higher *d-excess* values than those in a winter period (7.99). Moreover, the less variation in the seasonal cycle of *d-excess* (mean value of 6.28 ± 1.77‰) values signify the dominant moisture transport from the neighboring stationary ocean source (e.g. Jouzel and Merlivat, 1984; Jouzel and others, 2007; Fujita and Abe, 2006). Although the distribution of *d-excess* differed from the oscillations of $\delta^{18}O$ and δD, the relative consistency in the variation is likely to be linked to the dominant contribution of the steady marine source and local transport of the precipitation (Delmotte and others, 2000). It is because the variation of the sea surface temperature, relative humidity and wind speed at the moisture source region strongly control the variations of *d-excess* (Merlivat and Jouzel, 1979). Stenni and others (2000) suggested the main influences are originated from the Pacific Ocean sector and the Ross Sea.

3.1.2. Temporal variations of ionic compositions

The sea-salt (process of bubble bursting and wind blowing on the wave crests on open-water and ice-covered area) and oceanic biogenic activities are considered as two major sources of ionic species in the coastal Antarctic firn cores (e.g. Delmas and others, 1992; Wagenbach and others, 1998; Kreutz and Mayewski, 1999; Benassai and others, 2005). Higher concentrations of sea-salt aerosols (e.g. Na^+, Mg^{2+}, K^+, Ca^{2+}, Cl^- and $ssSO_4^{2-}$) are observed in the winter layer, related to the thin layer of sea-salt-enriched crystal formed above sea ice and its movement with blowing snow (Rankin and other, 2000; Abram and others, 2007; Jiayue and others, 2017; Vega and others, 2018), which is larger than those transported from open sea during warm periods. Coupled with high cyclonic activities in the Ross Sea, mineral dusts (partial of K^+, Mg^{2+} and Ca^{2+}) showed an enhancement in spring and summer in northern Victoria Land (e.g. Caiazzo and others, 2017). This relates to the input from local ice-free areas as well as long-range transport from South America (Kreutz and others, 1999). Na^+ is a more reliable proxy for sea-spray aerosol due to the absence of extra sources, particularly in coastal regions, and the steady concentration during transport

https://doi.org/10.1017/jog.2020.53 Published online by Cambridge University Press

and preservation without fractionation (Traversi and others, 2004).

In the firn core, Na^+ show increase in some winter period which may be associated with the high concentrations of sea-salt aerosols induced by the changes in sea ice and the intensive winter storm events, moving sea-salt aerosols (Brimblecombe, 1996; Udisti and others, 1998; Rankin and others, 2000; Stenni and others, 2000). According to the wind data from the Lola AWS (1990–2014), the higher velocities >30 m s^{-1} were observed mostly in late autumn to early spring (69% of total counts) and highest frequencies occurred in winter (between June and September) with 50.4% of the total counts. Moreover, the western and southwestern winds were dominant in these data, suggesting the air masses originated from ocean. However, the Na^+ concentration peaks as well as K^+ and Mg^{2+} were not consistent with all case in winter values (Fig. 2). It may indicate the event-based distribution relating to variability of atmospheric pressure pattern (e.g. Tuohy and others, 2015). The slope between the Na^+ and Cl^- ($[Cl^-] = 1.846 \times [Na^+] + 23.47$, $R^2 = 0.99$, $n = 197$, $p < 0.001$) was similar to the ratio in sea water (1.81), which represents the dominant contribution of the oceanic source (Traversi and others, 2004). However, with this intercept of 23.47 and the Cl^-/Na^+ ratio for each sample for each depth was larger than the sea-water ratio of 1.81 indicate the additional source for Cl^- (Benassai and others, 2005). Due to this inconsistent distribution trend of the sea-salt aerosols, we were not able to use them as time markers for age dating.

Shifts in the distribution of Ca^{2+} ions suggest contribution from various sources in this area. The average value of the nss fraction of Ca^{2+} is 74.0%, indicating the less dominantly sourced from sea spray. Other sources are considered as a crustal dust input to the total budget of Ca^{2+} (Fig. 2). Although, the high concentration of $nssCa^{2+}$ could indicate the spring and summer season due to the mesoscale cyclonic activities (Caiazzo and others, 2017) and generally lithophile elements are influenced by the wind events in the Ross Sea region (Rhodes and others, 2012). Our result shows no distinguishable seasonal pattern for Ca^{2+}, which thus cannot be used for age determination of the firn core.

Because the site is near to coast, $nssSO_4^{2-}$ is mainly derived from the marine biogenic activity (oxidation of dimethylsulfide [DMS] emitted from marine algae and phytoplankton) and partially from crustal erosion, and volcanic emissions (Handler, 1989; Delmas and others, 1992). Moreover, the spikes in $nssSO_4^{2-}$ indicate the timing of volcanic eruption in polar ice cores (e.g. Legrand and Mayewski, 1997; Cole-Dai and others, 1999). Together with the increased MSA, which was solely from marine biogenic activity, the values of $nssSO_4^{2-}$ and MSA illustrate noticeable signal of spring and summer snow layers in the northern Victoria Land (e.g. Legrand and others, 1992; Udisti and others, 1998; Saltzman and others, 2006; Rhodes and others, 2012; Becagli and others, 2016). The MSA and $nssSO_4^{2-}$ are observed with a similar concentration range to other studies (Stenni and others, 2000) and the maximum values are slightly differed from each other (Fig. 2). This discrepancy is likely to be linked to the distinct characteristic of the photochemical oxidation rate (Preunkert and others, 2008) and difference in the size and movement trajectory of them even both enhanced during the spring/summer period (Becagli and others, 2012). The MSA record reveals the weak correlation with $nssSO_4^{2-}$ ($r = 0.34$, $p < 0.001$, $n = 197$). The culmination values of $nssSO_4^{2-}$ and MSA were detected mostly in the late spring/summer before the summer maximum of $\delta^{18}O$ associated with the enrichment of marine biogenic activity with a presence of open-water area (Fig. 2) (e.g. Udisti and others, 1998; 1999; Stenni and others, 2000; Kwak and others, 2015). The spring/summer elevated values matched with the earlier studies (e.g. Whitlow and others, 1992; Stenni and others, 2000; Caiazzo and others, 2016).

The negative values of $nssSO_4^{2-}$, which are principally observed in coastal/low-latitude areas and detected at depths of 6.29 and 8.52 m in the firn core, is likely to be the winter high sea-spray content (Piccardi and others, 1996; Udisti and others, 1998). The $nssSO_4^{2-}$ concentration reached a maximum value of 523.0 μg L^{-1} at a depth of 8.04 m with relatively higher concentrations at the subsequent depth intervals (8.07–8.15 m), compared to the mean concentration of 48.5 μg L^{-1}. Moreover, this increasing trend with double peaks continues to the depth of 7.17 m with a relatively higher concentration of $nssSO_4^{2-}$ and the higher enrichment factor of SO_4^{2-} (Fig. 2).

We have assumed that the peak values at this depth range to be sourced from a volcanic eruption that occurred in 1991 (Stenni and others, 2002; Karlöf and others, 2005; Nardin and others, 2020). The Pinatubo eruption (June 1991, Philippines, 15°08′ N, 73°00′ E) released 18 ± 2 Mt SO_2 (Cole-Dai and others, 1999) and Cerro Hudson eruption (August 1991, Chile, 45°55′ S, 73°00′ W) (Legrand and Wagenbach, 1999) injected 2 Mt of SO_2 into the atmosphere (Doiron and others, 1991). In the previous studies, the Cerro Hudson plume was centered over the South pole in September 1991 and Pinatubo plume was indicated in November 1991 (Cacciani and others, 1993; Saxena and others, 1995). The annual layer counting revealed that the depth of the higher concentrations of $nssSO_4^{2-}$ (particularly at 7.61–7.84 m) corresponds to late-1992 to early-1994. This is sufficiently consistent with other studies, showing that the aerosol mass of Pinatubo spread in mid-1992 and late-August or early-September of 1992 (Trepte and others, 1993; Hitchman and others, 1994; Cole-Dai and others, 1999; Severi and others, 2009). Meanwhile, the depth range of 8.04–8.15 m with the sharp sulfate peak (late-1991 to early-1992) is likely to represent the volcanic aerosol input from the Cerro Hudson with the early detection associated with the relatively near distance to the site (e.g. Cole-Dai and others, 1999; Karlöf and others, 2005). This separate detection of two volcanic events was also observed in other sites (Cole-Dai and others, 1999; Stenni and others, 2002; Karlöf and others, 2005; Nardin and others, 2020) however there are some cases of single detection of only Pinatubo eruption (smooth peak) even in the site from northern Victoria Land (e.g. Severi and others, 2009). Thus, this result suggests the potential of the firn cores in this site to recover high-resolution records. Despite the potential local inputs from Mount Erebus (>300 km far from the Styx Glacier) and Mount Melbourne volcano (~40 km distance from the Styx Glacier), from this point of view, our findings confirm the notable $nssSO_4^{2-}$ value indicate volcanic signals as well as a seasonal indicator (spring/summer) with MSA for dating purposes.

3.4. Dating and accumulation rate

The annual signals of peak values ($\delta^{18}O$) with MSA and $nssSO_4^{2-}$ were observed in every 0.34 m (averagely eight samples per year for isotopic profile) in snow depth and suggest a 25-year record (1990–2014). The $nssSO_4^{2-}$ of the volcanic events (Pinatubo and Cerro Hudson) in 1991 was recognized in the time period between 1991 and 1994 in the dating scale. The dating difference is due to the transportation time of the volcanic gas to the high latitude sites in Antarctica (Legrand and Mayewski, 1997).

The density of the firn core ranged between 330 and 500 kg m^{-3} with increasing trend as depth increases. The annual mean accumulation rate was calculated by multiplying the snow density and was estimated to be 146 ± 60 kg m^{-2} a^{-1} (mean value ± std dev.) during the period of 1990 to 2014. The depth–age relationship by the layer counting method was plotted together with the densification model results in Figure 3. To compare the age by

https://doi.org/10.1017/jog.2020.53 Published online by Cambridge University Press

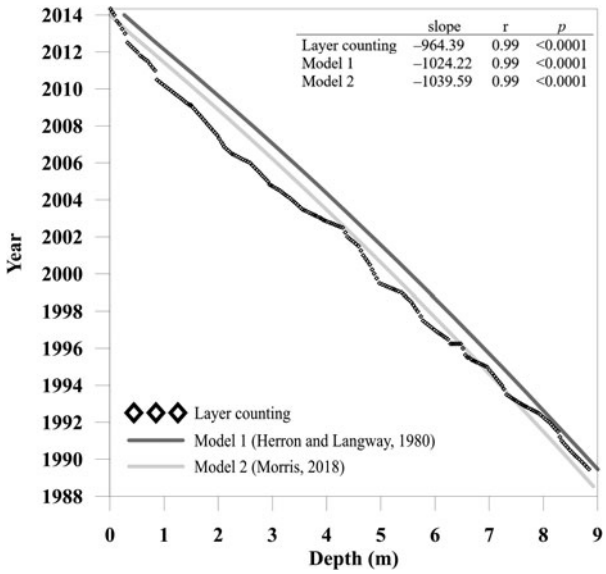

Fig. 3. The comparison of the depth–age relationship of the annual layer counting and the firn densification models.

annual layering method with the densification model, the depth values of the annual layering was converted to the same values of the models. Our estimate of annual mean accumulation rate is reasonable because there was an average value of 1.6- and 0.8-years difference with M1 and M2 ($n = 22$), respectively. Our estimate on annual mean snow accumulation is closer to the model-based estimation of 130 kg m^{-2} a^{-1} (Han and others, 2015) and comparable to other quantities of accumulation rate on Styx Glacier having values of 160, 203 and 226 kg m^{-2} a^{-1} (Udisti, 1996; Stenni and others, 2000; Kwak and others, 2015) (Table 3). Although the mean precipitation rate from ERA-Interim reanalysis (154 ± 37 kg m^{-2} a^{-1}) is similar to our estimated value (local estimate), the temporal variation of snow accumulation during the corresponding period was different (Fig. 4). This inconsistency in the annual accumulation rate can be resulted by the post-depositional effects, including mainly by the wind-driven snow redistribution and partially by the no existence of precipitation, surface and snowdrift sublimation in snow layers (Fig. 4) (e.g. Frezzotti and others, 2004; Karlöf and others, 2005; Sinclair and others, 2010; Rhodes and others, 2012), and the influence by the temperature change, regime of precipitation and changes in cyclonic systems (e.g. frequency, path, timing and strength) (Kreutz and others, 2000; Goodwin and others, 2003; Kaspari and others, 2004). Jang and others (2019) have mentioned that the strong wind effect (as blizzards) could have induced the large variation in density of snow in the Styx Glacier.

Stenni and others (2000) reported the annual accumulation range of 111–335 kg m^{-2} a^{-1} for the period between 1971 and 1990 and this estimation is plotted together with the firn core (Fig. 4). There is an overall decreasing trend in accumulation rate in our estimate ($r = -0.53$, $p < 0.001$, $n = 25$). The accumulation profile was expanded with Stenni and others (2000) ($r = -0.56$, $p < 0.001$, $n = 45$). The highest (>200 kg m^{-2} a^{-1}) annual accumulation rate was observed in years 1992, 1995, 1996, 1999, 2002 to 2004, while the three lowest annual accumulation rates occurred during 2012–2014. Stenni and others (2000) highlighted that there was an important role of the Ross Sea SIE on the snow precipitation in northern Victoria Land. The mean SIE in the Ross Sea region during cold period (months between June and November [JJASON]) shows a weak negative correlation with both the snow accumulation rate ($r = -0.41$, $p < 0.01$, $n = 25$) and an annual mean $\delta^{18}O$ ($r = -0.32$, $p < 0.05$, $n = 25$) of the firn core.

A negative correlation between *d-excess* and SIE was observed with a correlation coefficient of −0.53 between *d-excess* record of the WhiteHall Glacier site and SIE of the Ross Sea (Sinclair and others, 2014). However, we find a weaker correlation between our *d-excess* and the SIE ($r = -0.21$, $p < 0.01$, $n = 25$) as well as a weak negative correlation of SIE with the annual flux of MSA ($r = -0.51$, $p < 0.01$, $n = 25$) and nssSO_4^{2-} ($r = -0.39$, $p < 0.01$, $n = 25$), while the annual flux of Na^+ does not show significant correlation (Fig. 4). It can be explained by single strong source of open-water area for the emission of DMS to the concentrations of MSA and nssSO_4^{2-} (e.g. Rhodes and others, 2009; Sinclair and others, 2014). While several enhancing factors (may likely to individual storm events) rather than only SIE was assumed for the Na^+ concentration in the firn core. The increasing (trend) of SIE during the period of 1990 to 2014 in the Ross sea region and evidence in ice core from WhiteHall Glacier (Sinclair and others, 2014) and decreasing precipitation from the firn core is likely to be coupled with the positive trend of Southern Annular Mode (Marshall and others, 2018) and deepening of Amundsen Sea Low pressure and its location (Hosking and others, 2013; Sinclair and others, 2014), which enhances westerly winds and the cooling of air temperature (−0.55 ± 0.97°C/100 a^{-1}) in the northern Victoria Land coast (Stenni and others, 2017; Yang and others, 2018).

With respect to the conventional correlation of annual mean values of isotopic ratio and air temperature ($T - \delta^{18}O$) (Dansgaard, 1964; Petit and others, 1999), the isotopic composition of the firn core does not quantitatively represent this relationship with temperature record of both Lola AWS and ERA-Interim due to the alteration of seasonality of $\delta^{18}O$ with increasing depth and coupled influencing factors (Fig. 4). Annual mean $\delta^{18}O$ (δD) fluctuated between −40.65‰ (−320.9‰) and −30.24‰ (−236.1‰) with a mean of −34.96‰ (−273.6‰) and std dev. of 2.17‰ (17.68‰), while the atmospheric temperature measured at the nearest Lola AWS was less variated (ranged between −23.41 and −18.83°C with the mean of −22.44°C and std dev. of 1.02°C). Stenni and others (2000) compiled the annual mean temperature (both AWS and borehole temperature measurement) and mean $\delta^{18}O$ values from other firn cores in northern Victoria Land and suggests a slope of 0.81‰ °C^{-1} ($r = 0.9$). Slightly different slopes of 0.44‰ °C^{-1} (van Ommen and Morgan, 1997), 0.60‰ °C^{-1} (Stenni and others, 2002) and 0.62‰ °C^{-1} (Sinclair and others, 2012) were reported in East Antarctic sites. Moreover, Stenni and others (2017) reported a slope of 1.05‰ °C^{-1} in East Antarctic Plateau and 1.21‰ °C^{-1} in Victoria Land coast by model simulation.

In our study, the gradients of 1.07 and 1.20‰ °C^{-1} were found by comparing mean $\delta^{18}O$ value (−34.96‰) with borehole temperature (−32.5°C) and mean annual temperature from ERA-Interim (−29.07°C), respectively. Large difference in mean temperature recorded in the Lola AWS (−22.44°C) compared to the estimates in borehole and ERA-Interim suggests the importance of a reliable instrumental records. The various factors including changes in evaporation conditions, transport pathway, and changes in precipitation seasonality (Werner and others, 2018) and post-depositional processes (Sinclair and others, 2010; Rhodes and others, 2012; Goursaud and others, 2017; Casado and others, 2018) need to be considered to this high-resolution firn core record. Moreover, there are studies that reported a weak or no correlation between annual mean temperature and $\delta^{18}O$ in the coastal Antarctic sites (Bertler and others, 2011, 2018; Goursaud and others, 2019). Goursaud and others (2018) suggested challenges to obtain a correlation between annual mean temperature and $\delta^{18}O$ by the ECHAM5-wiso simulation during the period between 1979 and 2013. With the consideration of short-temporal data for comparison, at this stage the

https://doi.org/10.1017/jog.2020.53 Published online by Cambridge University Press

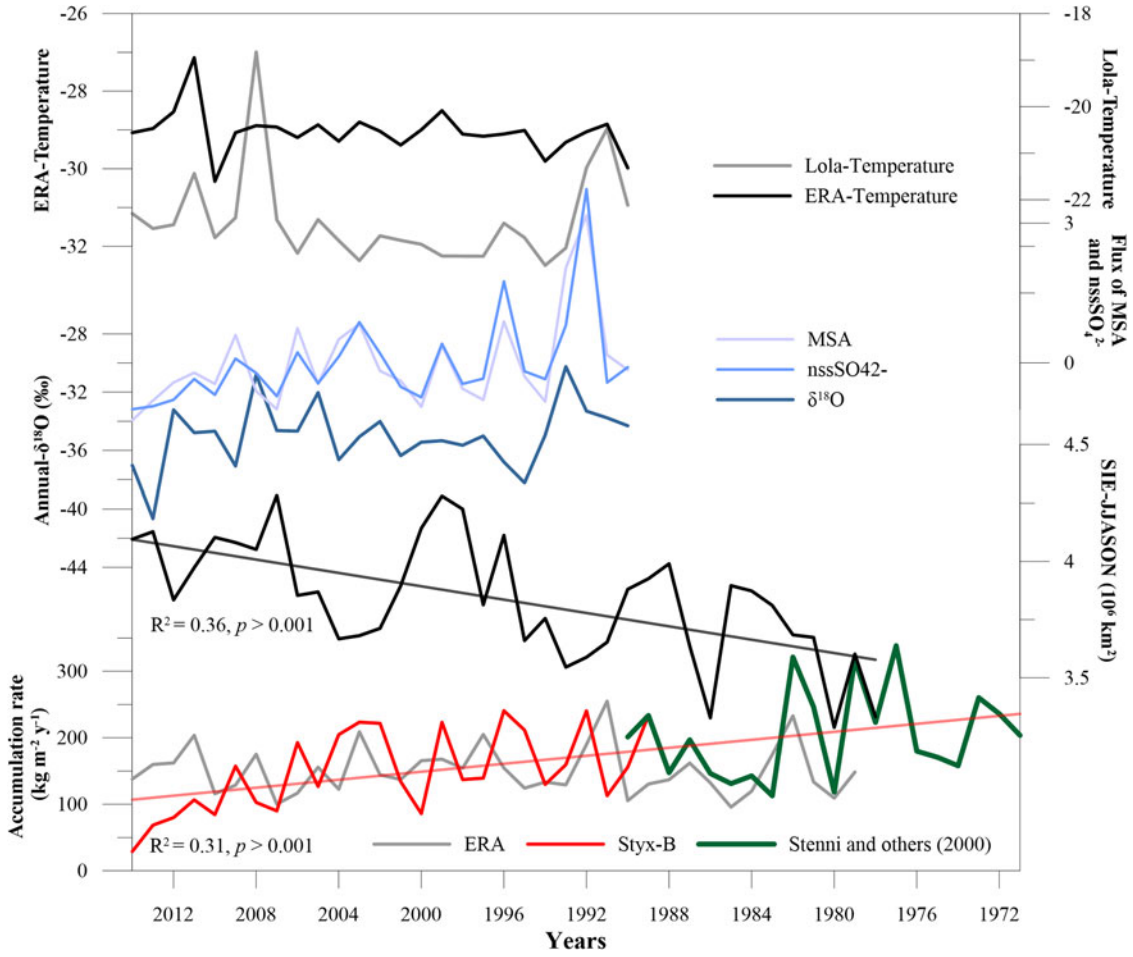

Fig. 4. Comparison of annual accumulation rate (Styx-B firn core, ERA-Interim, Stenni and others, 2000), annual mean $\delta^{18}O$, standardized annual flux of MSA and $nssSO_4^{2-}$, SIE during cold period (JJASON) and temperature record from Lola AWS and ERA-Interim reanalysis data. The linear trendlines shown for annual accumulation rate (Styx-B firn core for the period of 1990–2014 together with Stenni and others (2000) up to 1971 from 1990) and trend of SIE between 1979 and 2014.

Table 3. Mean accumulation rates estimated near to the Styx Glacier for comparison to the firn core

Locations	Accumulation rate, kg m^{-2} a^{-1}	Time period	Reference
Styx Glacier	146 ± 60	1990–2014	This study
ERA-Interim	154 ± 37	1990–2014	Dee and others, 2011
ERA-Interim	150 ± 36	1979–2014	
Hercules Neve	160	1971–1992	Udisti (1996)
Styx Glacier	203 (111–335)	1971–1990	Stenni and others (2000)
Talos Dome	86.6	1965–2007	Stenni and others (2002)
Styx Glacier	226	2009–2012	Kwak and others (2015)
Styx-M (densification model for Styx-M-core)	130	~1360–2014	Han and others (2015)
GV7	242 ± 71	2008–2013	Caiazzo and others (2017)

isotopic and ionic species (MSA and $nssSO_4^{2-}$) of the firn core are likely to preserve the sign of oceanic environment. This study can be applied for the interpretation of the longer ice core drilled at the same site which is being in analysis.

4. Summary

The chronology of the firn core from Styx Glacier in northern Victoria Land, Antarctica was studied through the temporal variations of its isotopic and ionic compositions to estimate the snow accumulation rate. The seasonal variations of $\delta^{18}O$, MSA and $nssSO_4^{2-}$ which represent the ocean-sourced precipitation and reference horizon of volcanic sulfate signal were used to identify the age of the firn core. The 25 annual signals spanning back from 1990 to 2014 were measured with a mean accumulation rate of 146 ± 60 kg m^{-2} a^{-1}. A decreasing trend of the accumulation was observed through the profile. The annual mean accumulation rate and $\delta^{18}O$, flux of MSA and $nssSO_4^{2-}$ were shown to be correlated with sea-ice extent (JJASON) in the Ross Sea region. Although the records are short, at this stage this site is likely to preserve the changes in oceanic environment which also can be confirmed in the long ice core. This study will be useful for the interpretation of long ice core drilled at the same site.

Acknowledgements. This study was supported by the Basic Science Research Program through the National Research Foundation of Korea (NRF) funded by the Ministry of Education (2017R1D1A1A09000732) and KOPRI research grant (PE20190). We thank Dr. Elizabeth Morris for sharing the results of firn densification models and comments on the manuscript. We are also grateful to the Italian PNRA (Programma Nazionale di Ricerche in Antartide) project for providing meteorological data from Lola AWS (http://www.climantartide.it) and the ERA-Interim dataset from the ECMWF. We appreciate the scientific editor and two anonymous reviewers, whose comments led to significant improvements.

References

Abram NJ, Mulvaney R, Wolff EW and Mudelsee M (2007) Ice core records as sea ice proxies: an evaluation from the Weddell Sea region of Antarctica. *Journal of Geophysical Research-Atmospheres* **112**, D15101. doi: 10.1029/2006JD008139.

Anderson DL and Benson CS (1963) The densification and diagenesis of snow. In Kingery W, ed. *Ice and Snow; Properties, Processes, and Applications*; Proceedings of a conference held at the Massachusetts Institute of Technology. February 12–16, 1962. Cambridge, Mass., M.I.T. Press, pp. 391–411.

Anschütz H and 8 others (2011) Variation of accumulation rates over the last eight centuries on the East Antarctic Plateau derived from volcanic signals in ice cores. *Journal of Geophysical Research* **116**, D20103. doi: 10.1029/2011JD015753, 2011.

Becagli S and 10 others (2012) Study of present-day sources and transport processes affecting oxidized sulphur compounds in atmospheric aerosols at Dome C (Antarctica) from year-round sampling campaigns. *Atmospheric Environment* **52**, 98–108. doi: 10.1016/j.atmosenv.2011.07.053.

Becagli S and 18 others (2016) Relationships linking primary production, sea ice melting, and biogenic aerosol in the Arctic. *Atmospheric Environment* **136**, 1–15.

Benassai S and 6 others (2005) Sea-spray deposition in Antarctic coastal and plateau areas from ITASE traverses. *Annals of Glaciology* **41**, 32–40. doi: 10.3189/172756405781813285.

Benson CS (1962) Stratigraphic studies in the snow and firn of the Greenland ice sheet. SIPRE. *Research Report* **70**, 1–93.

Bertler NAN and 72 others (2018) The Ross Sea dipole – temperature, snow accumulation and sea ice variability in the Ross Sea region, Antarctica, over the past 2700 years. *Climate of the Past* **14**, 193–214, doi: 10.5194/cp-14-193-2018, 2018.

Bertler NAN, Mayewski P and Carter L (2011) Cold conditions in Antarctica during the Little Ice Age – implications for abrupt climate change mechanisms. *Earth and Planetary Science Letters* **308**, 41–51, 2011.

Brimblecombe P (1996) *Air Composition and Chemistry*. Cambridge: Cambridge University Press.

Bromwich DH and Weaver CJ (1983) Latitudinal displacement from main moisture source controls $\delta^{18}O$ of snow in coastal Antarctica. *Nature* **301** (5896), 145–147.

Cacciani M, Girolamo PD, di Sarra A, Fiocco G and Fu D (1993) Volcanic aerosolayers observed at South Pole, September 1991–June 1992. *Geophysical Research Letters* **20**, 807–810.

Caiazzo L and 6 others (2016) Spatial and temporal variability of snow chemical composition and accumulation rate at Talos Dome site (East Antarctica). *Science of the Total Environment* **550**, 418–430. doi: 10.1016/j.scitotenv.2016.01.087.

Caiazzo L and 25 others (2017) Prominent features in isotopic, chemical and dust stratigraphies from coastal East Antarctic ice sheet (Eastern Wilkes Land). *Chemosphere* **176**, 273–287.

Casado M and 12 others (2018) Archival processes of the water stable isotope signal in East Antarctic ice cores. *The Cryosphere* **12**, 1745–1766. doi: 10.5194/tc-12-1745-2018.

Cole-Dai J, Mosley-Thompson E and Qin D (1999) Evidence of the 1991 Pinatubo volcanic eruption in South Polar snow. *Chinese Science Bulletin* **44**,756. doi: 10.1007/BF02909720.

Dansgaard W (1964) Stable isotopes in precipitation. *Tellus* **16**(4), 436–468. doi: 10.3402/tellusa.v16i4.8993.

Dee DP and 35 others (2011) The ERA-Interim reanalysis: configuration and performance of the data assimilation system. *Quarterly Journal of the Royal Meteorological Society* **137** (656), 553–597.

Delmas RJ, Kirchner S, Palais JM and Petit JR (1992) 1000 Years of explosive volcanism recorded at the South Pole. *Tellus B* **44**, 335–350. doi: 10.1034/j.1600-0889.1992.00011.x.

Delmotte M, Masson V, Jouzel J and Morgan VI (2000) A seasonal deuterium excess signal at Law Dome, coastal eastern Antarctica: a Southern Ocean signature. *Journal of Geophysical Research Atmospheres* **105**(D6), 7187–7197. doi: 10.1029/1999JD901085.

Doiron SD, Bluth GJS, Schnetzler CC, Krueger AJ and Walter LS (1991) Transport of Cerro Hudson SO_2 clouds. *Eos Transactions American Geophysical Union* **72**(45), 489–498. doi: 10.1029/90EO00354.

Drewry DJ, Jordan SR and Jankowski E (1982) Measured properties of the Antarctic ice sheer: surface configuration, ice thickness, volume and bedrock characteristics. *Annals of Glaciology* **3**, 83–91.

Frezzotti M and 13 others (2004) New estimations of precipitation and surface sublimation in East Antarctica from snow accumulation measurements. *Climate Dynamics* **23**, 803–813.

Frezzotti M, Urbini S, Proposito M, Scarchilli C and Gandolfi S (2007) Spatial and temporal variability of surface mass balance near Talos Dome, East Antarctica. *Journal of Geophysical Research* **112**, F02032. doi: 10.1029/2006JF000638.

Fujita K and Abe O (2006) Stable isotopes in daily precipitation at Dome Fuji, East Antarctica, *Geophysical Research Letters* **33**, L18503. doi: 10.1029/2006GL026936.

Furukawa R and 6 others (2017) Seasonal-scale dating of a shallow ice core from Greenland using oxygen isotope matching between data and simulation. *Journal of Geophysical Research: Atmospheres* **122**, 10873–10887. doi: 10.1002/2017JD026716.

Goodwin I, de Angelis M, Pook M and Young NW (2003) Snow accumulation variability in Wilkes Land, East Antarctica, and the relationship to atmospheric ridging in the 130°–170°E region since 1930. *Journal of Geophysical Research* **108**, 4673. doi: 10.1029/2002JD002995.

Goursaud S and 10 others (2017) A 60-year ice-core record of regional climate from Adélie Land, coastal Antarctica. *The Cryosphere* **11**, 343–362. doi: 10.5194/tc-11-343-2017.

Goursaud S and 6 others (2019) Challenges associated with the climatic interpretation of water stable isotope records from a highly resolved firn core from Adélie Land, coastal Antarctica. *The Cryosphere* **13**, 1297–1324. doi: 10.5194/tc-13-1297-2019, 2019.

Goursaud S, Masson-Delmotte V, Favier V, Orsi A and Werner M (2018) Water stable isotope spatio-temporal variability in Antarctica in 1960–2013: observations and simulations from the ECHAM5-wiso atmospheric general circulation model. *Climate of the Past* **14**, 923–946. doi: 10.5194/cp-14-923-2018, 2018.

Han YC and 7 others (2015) Shallow ice-core drilling on Styx glacier, northern Victoria Land, Antarctica in the 2014–2015 summer. *Journal of the Geological Society of Korea* **51**(3), 343–355.

Handler P (1989) The effect of volcanic aerosols on global climate. *Journal Volcanology and Geothermal Research* **37**(3-4), 233–249. doi: 10.1016/0377-0273(89)90081-4.

Herron M and Langway C (1980) Firn densification: an empirical model. *Journal of Glaciology* **25**(93), 373–385. doi: 10.3189/S0022143000015239.

Hitchman MH, McKay M and Trepte C R (1994) A climatology of stratospheric aerosol. *Journal of Geophysical Research* **99**, 20689.

Holloway M, Sime L and Singarayer J (2016) Antarctic last interglacial isotope peak in response to sea ice retreat not ice-sheet collapse. *Nature Communication* **7**, 12293. doi: 10.1038/ncomms12293.

Hong SB and 6 others (2012) Uncertainties of ionic species in snowpit samples determined with ion chromatography system. *Analytical Science and Technology of Korea* **25**(6), 350–363.

Hoshina Y, Fujita K, Iizuka Y and H and Motoyama (2016) Inconsistent relationships between major ions and water stable isotopes in Antarctic snow under different accumulation environments. *Polar Science* **10**(1), 1–10. doi: 10.1016/j.polar.2015.12.003.

Hosking JS, Orr A, Marshall GJ, Turner J and Phillips T (2013) The influence of the Amundsen–Bellingshausen Seas low on the climate of West Antarctica and its representation in coupled climate model simulations. *Journal of Climate* **26**, 6633–6648. doi: 10.1175/JCLI-D-12-00813.1.

Hur SD (2013) *Development of Core Technology for Ice Core Drilling and Ice Core Bank (Rep. BSPE13070–037-7)*. Incheon: Korea Polar Research Institute.

Jang and 14 others (2019) Very old firn air linked to strong density layering at Styx Glacier, coastal Victoria Land, East Antarctica. *The Cryosphere* **13**, 2407–2419. doi: 10.5194/tc-13-2407-2019, 2019.

Jiayue H and Lyatt J (2017) Wintertime enhancements of sea salt aerosol in polar regions consistent with a sea ice source from blowing snow. *Atmospheric Chemistry and Physics* **17**, 3699–3712.

Johnsen SJ and 5 others (2000) Diffusion of stable isotopes in polar firn and ice: the isotope effect in firn diffusion. *Physics of Ice Core Records.*, **159**, 121–140.

Jones J and 24 others (2016) Assessing recent trends in high-latitude Southern Hemisphere surface climate. *Nature Climate Change* **6**, 917–926. doi: 10.1038/nclimate3103.

Jouzel J and 6 others (1997) Validity of the temperature reconstruction from water isotopes in ice cores. *Journal of Geophysical Research* **102**(C12), 26471–26487. doi: 10.1029/97JC01283.

Jouzel J and 31 others (2007) Orbital and millennial Antarctic climate variability over the past 800000 years. *Science* **317**(5839), 793–796. doi: 10.1126/science.1141038.

Jouzel J and Masson-Delmotte V (2010) Paleoclimates: what do we learn from deep ice cores? *WIREs Climate Change* **1**(5), 654–669. doi: 10.1002/wcc.72.

https://doi.org/10.1017/jog.2020.53 Published online by Cambridge University Press

Jouzel J and Merlivat L (1984) Deuterium and oxygen 18 in precipitation: modeling of the isotope effects during snow formation. *Journal of Geophysical Research*, **89**, 11749–11757.

Karlöf L and 11 others (2005) Accumulation variability over a small area in east Dronning Maud Land, Antarctica, as determined from shallow firn cores and snow pits: some implications for ice-core records. *Journal of Glaciology* **51**(174), 343–352. doi: 10.3189/172756505781829232.

Kaspari S and 6 others (2004) Climate variability in West Antarctica derived from annual accumulation-rate records from ITASE firn/ice cores. *Annals of Glaciology* **39**, 585–594.

Knüsel S, Brütsch S, Henderson KA, Palmer AS and Schwikowski M (2005) ENSO Signals of the twentieth century in an ice core from Nevado Illimani, Bolivia. *Journal of Geophysical Research* **110**, D01102. doi: 10.1029/2004JD005420.

Kreutz KK and 5 others (2000) Sea level pressure variability in the Amundsen Sea region inferred from a West Antarctic glaciochemical record. *Journal of Geophysical Research: Atmosphere* **105**(D3), 4047–4059.

Kreutz KJ and Mayewski PA (1999) Spatial variability of Antarctic surfaces snow glaciochemistry: implications for paleoatmospheric circulation reconstructions. *Antarctic Science* **11**, 105–118.

Krinner G, Magand O, Simmonds I, Genthon C and Dufresne JL (2007) Simulated Antarctic precipitation and surface mass balance at the end of the twentieth and twenty-first centuries. *Climate Dynamics* **28**, 215–230.

Kuramoto T and 6 others (2011) Seasonal variations of snow chemistry at NEEM, Greenland. *Annals of Glaciology* **52**(58), 193–200. doi: 10.3189/172756411797252365.

Kwak H and 6 others (2015) A study on high-resolution seasonal variations of major ionic species in recent snow near the Antarctic Jang Bogo Station. *Ocean & Polar Research* **37**(2),127–140. doi: 10.4217/OPR.2015.37.2.127.

Lee J and 6 others (2010) Isotopic evolution of a seasonal snowcover and its melt by isotopic exchange between liquid water and ice. *Chemical Geology* **270**, 126–134.

Lee J, Ko K, Kim J and Chang H (2008) Multivariate statistical analysis of underground gas storage caverns on groundwater chemistry in Korea. *Hydrological Processes* **22**, 3410–3417. doi: 10.1002/hyp.6921.

Legrand M, Feniet-Saigne C, Saltzman ES and Germain C (1992) Spatial and temporal variations of methanesulfonic acid and nonsea salt sulfate in Antarctic ice. *Journal of Atmospheric Chemistry* **14**, 245–260. doi: 10.1007/BF00115237.

Legrand M and Mayewski P (1997) Glaciochemistry of polar ice cores: a review. *Review of Geophysics* **35**(3), 219–243. doi: 10.1029/96RG03527.

Legrand M and Wagenbach D (1999) Impact of the Cerro Hudson and Pinatubo volcanic eruptions on the Antarctic air and snow chemistry. *Journal of Geophysical Research* **104**(D1), 1581–1596. doi: 10.1029/1998JD100032.

Maggi V and 6 others (1998) 70 Years of northern Victoria L and (Antarctica) accumulation rate. *Annals of Glaciology* **27**, 215–219. doi: 10.3189/1998AoG27-1-215-219.

Markle BR, Bertler NAN, Sinclair KE and Sneed SB (2012) Synoptic variability in the Ross Sea region, Antarctica, as seen from back-trajectory modeling and ice core analysis. *Journal of Geophysical Research* **117**, 1–17. doi: 10.1029/2011JD016437.

Marshall G and National Center for Atmospheric Research Staff (Eds) (2018) Last modified 19 Mar 2018. The Climate Data Guide: Marshall Southern Annular Mode (SAM) Index (Station-based). Available at https://climatedataguide.ucar.edu/climate-data/marshall-southern-annular-mode-sam-index-station-based.

Masson-Delmotte V and 35 others (2008) A review of Antarctic surface snow isotopic composition: observations, atmospheric circulation, and isotopic modeling. *Journal of Climate* **21**, 3359–3387. doi: 10.1175/2007JCLI2139.1.

Merlivat L and Jouzel J (1979) Global climatic interpretation of the deuterium-oxygen 18 relationship for precipitation. *Journal of Geophysical Research* **84**(C8), 5029–5033. doi: 10.1029/JC084iC08p05029.

Morris E (2018) Modeling dry-snow densification without abrupt transition. *Geosciences* **8**, 464. doi: 10.3390/geosciences8120464.

Nardin R and 7 others (2020) Volcanic fluxes over the last millennium as recorded in the Gv7 ice core (Northern Victoria Land, Antarctica). *Geosciences* **10**, 38.

Noone D and Simmonds I (2004) Sea ice control of water isotope transport to Antarctica and implications for ice core interpretation. *Journal of Geophysical Research* **109**, D07105. doi: 10.1029/2003JD004228.

Parkinson CL and Cavalieri DJ (2012) Antarctic sea ice variability and trends, 1979–2010. *The Cryosphere* **6**, 871–880. doi: 10.5194/tc-6-871-2012.

Petit JR and 6 others (1999) Climate and atmospheric history of the past 420,000 years from the Vostok ice core, Antarctica. *Nature* **399**(6735), 429–436. doi: 10.1038/20859.

Piccardi G, Becagli S, Traversi R and Udisti R (1996) Fractionating phenomena, altitude induced, on snow composition in northern Victoria Land (Antarctica). In Calacino, M., G Giovannelli and 1. Stefanutti, eds. *Conference on Italian Research on Antarctic Atmosphere*, 6–8 November 1995, Florence, Italy. Proceedings, 5, Bologna, Societa Italiana di Fisica, 229–245.

Piccardi G, Udisti R and Casella F (1994) Seasonal trends and chemical composition of snow at Terra Nova Bay (Antarctica). *International Journal of Environmental Analytical Chemistry* **55**, 219–234.

Pilson MEQ (2013) *An Introduction to the Chemistry of the Sea*, 2nd Edn. New York: Cambridge University Press, 529.

Preunkert S and 5 others (2008) Seasonality of sulfur species (dimethylsulfide, sulfate, and methanesulfonate) in Antarctica: inland versus coastal regions. *Journal of Geophysical Research* **113**, D15302. doi: 10.1029/2008JD009937.

Rankin AM, Auld V and Wolff EW (2000) Frost flowers as a source of fractionated sea salt aerosol in the polar regions. *Geophysical Research Letters* **27**(21), 3469–3472.

Rhodes RH and 5 others (2009) Sea ice variability and primary productivity in the Ross Sea, Antarctica, from methylsulphonate snow record. *Geophysical Research Letters* **36**, L10704. doi: 10.1029/2009gl037311.

Rhodes RH and 6 others (2012) Little Ice Age climate and oceanic conditions of the Ross Sea, Antarctica from a coastal ice core record. *Climate of the Past* **8**, 1223–1238. doi: 10.5194/cp-8-1223-2012, 2012.

Rignot E, Velicogna I, van den Broeke MR, Monaghan A and Lenaerts J (2011) Acceleration of the contribution of the Greenland and Antarctic ice sheets to sea level rise. *Geophysical Research Letters* **38**, L05503. doi: 10.1029/2011GL046583.

Saltzman ES, Dioumaeva I and Finley BD (2006) Glacial/interglacial variations in methanesulfonate (MSA) in the Siple Dome ice core, West Antarctica. *Geophysical Research Letters* **33**, L11811. doi: 10.1029/2005GL025629.

Saxena VK, Anderson J and Lin NH (1995) Changes in Antarctic stratospheric aerosol characteristics due to volcanic eruptions as monitored by the Stratospheric Aerosol and Gas Experiment II satellite. *Journal of Geophysical Research* **100**(D8), 16,735–16,751.

Scarchilli C, Frezzotti M and Ruti PM (2011) Snow precipitation at four ice core sites in east Antarctica: provenance, seasonality and blocking factors. *Climate Dynamics* **37**, 2107–2125.

Severi M and 5 others (2009) Thirty years of snow deposition at Talos Dome (Northern Victoria Land, East Antarctica): chemical profiles and climatic implications. *Microchemical Journal* **92**, 15–20.

Sinclair KE, Bertler NAN, Bowen MM and Arrigo KR (2014) Twentieth century sea-ice trends in the Ross Sea from a high-resolution, coastal ice-core record. *Geophysical Research Letters* **41**, 1–7. doi: 10.1002/2014GL059821.

Sinclair KE, Bertler NAN and Trompetter WJ (2010) Synoptic controls on precipitation pathways and snow delivery to high-accumulation ice core sites in the Ross Sea region, Antarctica. *Journal of Geophysical Research* **115**, D22112. doi: 10.1029/2010JD014383.

Sinclair KE, Bertler NA and van Ommen TD (2012) Twentieth-century surface temperature trends in the Western Ross Sea, Antarctica: evidence from a high-resolution ice core. *Journal of Climate* **25**, 3629–3636. doi: 10.1175/JCLI-D-11-00496.1.

Steen-Larsen HC and 18 others (2014) What controls the isotopic composition of Greenland surface snow? *Climate of the Past* **10**, 377–392. doi: 10.5194/cp-10-377-2014.

Stenni B and 8 others (1999) 200 Years of isotope and chemical records in a firn core from Hercules Névé, Northern Victoria Land, Antarctica. *Annals of Glaciology* **29**, 106–112. doi: 10.3189/172756499781821175.

Stenni B and 6 others (2000) Snow accumulation rates in northern Victoria Land, Antarctica, by firn-core analysis. *Journal of Glaciology* **46**(155), 541–552.

Stenni B and 6 others (2002) Eight centuries of volcanic signal and climate change at Talos Dome (East Antarctica). *Journal of Geophysical Research* **107**(D9), 1–14. doi: 10.1029/2000JD000317.

Stenni B and 18 others (2017) Antarctic climate variability on regional and continental scales over the last 2000 years. *Climate of the Past* **13**, 1609–1634. doi: 10.5194/cp-13-1609-2017.

Thomas ER and 8 others (2019) Antarctic sea ice proxies from marine and ice core archives suitable for reconstructing sea ice over the past 2000 years. *Geosciences* **9**, 506.

https://doi.org/10.1017/jog.2020.53 Published online by Cambridge University Press

Traversi R and 6 others (2004) Spatial and temporal distribution of environmental markers from coastal to plateau areas in Antarctica by firn core chemical analysis. *International Journal of Environmental Analytical Chemistry* **84**(6–7), 457–470. doi: 10.1080/03067310310001640393.

Traversi R, Becagli S, Castellano E, Largiuni O and Udisti R (2000) Stability of chemical species in firn layers from Antarctica. In Colacino M and Giovannelli G (eds), *8th Workshop, Italian Research on the Antarctic Atmosphere. Proceedings*, vol. **69**. Bologna: Società Italiana di Fisica, pp. 421–443.

Trepte CR, Veiga RE and McCormick MP (1993) The poleward dispersal of Mt. Pinatubo volcanic aerosol. *Journal of Geophysical Research* **98**, 18563.

Tuohy A and 6 others (2015) Transport and deposition of heavy metals in the Ross Sea Region, Antarctica. *Journal of Geophysical Research: Atmosphere* **120**, 10,996–11,011. doi: 10.1002/2015JD023293.

Udisti R (1996) Multiparametric approach for chemical dating of snow layers from Antarctica. *International Journal of Environmental Analytical Chemistry* **63**, 225–244.

Udisti R and 6 others (1999) Chemical characterisation of a volcanic event (about AD 1500) at Styx Glacier plateau, northern Victoria Land, Antarctica. *Annals of Glaciology* **29**, 113–120. doi: 10.3189/172756499781821265.

Udisti R, Traversi R, Becagli G and Piccardi G (1998) Spatial distribution and seasonal pattern of biogenic sulphur compounds in snow from northern Victoria Land, Antarctica R. *Annals of Glaciology* **27**, 535–542.

van Ommen TD and Morgan VI (1997) Calibrating the ice core paleothermometer using seasonality. *Journal of Geophysical Research* **102**, 9351–9357.

Vega CP and 7 others (2018) Variability of sea salts in ice and firn cores from fimbul ice shelf, dronning maud land, Antarctica. *The Cryosphere* **2018**, 12, 1681–1697.

Wagenbach D, Legrand M, Fischer H, Pichlmayer F and Wolff EW (1998) Atmospheric near-surface nitrate at coastal Antarctic sites. *Journal of Geophysical Research: Atmospheres* **103.D9**(1998), 11007–11020.

Wagnon P, Delmas RJ and Legrand M (1999) Loss of volatile acid species from upper firn layers at Vostok, Antarctica. *Journal of Geophysical Research: Atmospheres* **104**(D3), 3423–3431. doi: 10.1029/98JD02855.

Werner M, Jouzel J, Masson-Delmotte V and Lohmann G (2018) Reconciling glacial Antarctic water stable isotopes with ice sheet topography and the isotopic paleothermometer. *Nature Communications* **9**, 3537.

Whitlow S, Mayewski PA and Dibb JE (1992) A comparison of major chemical species seasonal concentration and accumulation at the South Pole and summit, Greenland. *Atmospheric Environment. Part A. General Topics* **26** (11), 2045–2054. doi: 10.1016/0960-1686(92)90089-4.

Yang J-W and 10 others (2018) Surface temperature in twentieth century at the Styx Glacier, northern Victoria Land, Antarctica, from borehole thermometry. *Geophysical Research Letters* **45**, 9834–9842. doi: 10.1029/2018GL078770.

https://doi.org/10.1017/jog.2020.53 Published online by Cambridge University Press